

## Thermally Induced PCET

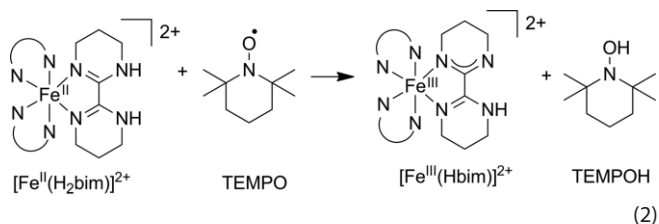
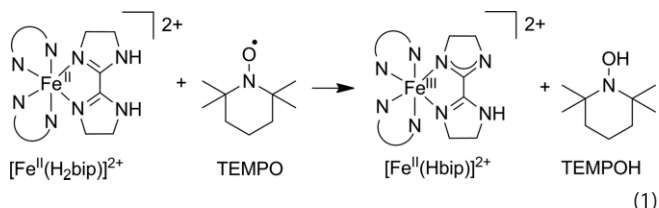
Thermally Induced Oxidation of  $[\text{Fe}^{\text{II}}(\text{tacn})_2](\text{OTf})_2$   
(tacn = 1,4,7-triazacyclononane)Jia Li,<sup>[a]</sup> Atanu Banerjee,<sup>[a]</sup> Debra R. Preston,<sup>[a]</sup> Brian J. Shay,<sup>[b]</sup> Amitiva Adhikary,<sup>[a]</sup>  
Michael D. Sevilla,<sup>[a]</sup> Reza Loloee,<sup>[c]</sup> Richard J. Staples,<sup>[d]</sup> and Ferman A. Chavez\*<sup>[a]</sup>

**Abstract:** We previously reported the spin-crossover (SC) properties of  $[\text{Fe}^{\text{II}}(\text{tacn})_2](\text{OTf})_2$  (**1**) (tacn = 1,4,7-triazacyclononane). Upon heating under dynamic vacuum, **1** undergoes oxidation to generate a low-spin iron(III) complex. The oxidation of the iron center was found to be facilitated by initial oxidation of the ligand through loss of a H atom. The resulting complex was hypothesized to have the formulation  $[\text{Fe}^{\text{III}}(\text{tacn})(\text{tacn-H})](\text{OTf})_2$  (**2**) where tacn-H is *N*-deprotonated tacn. The formulation was confirmed by ESI-MS. The powder EPR spectrum of the oxidized product at 77 K reveals the formation of a low-spin iron(III) species with rhombic spectrum ( $g = 1.98, 2.10, 2.19$ ). We have indirectly detected  $\text{H}_2$  formation during the heating of **1** by react-

ing the headspace with HgO. Formation of water ( $^1\text{H}$  NMR in anhydrous  $[\text{D}_6]\text{DMSO}$ ) and elemental mercury were observed. To further support this claim, we independently synthesized  $[\text{Fe}^{\text{III}}(\text{tacn})_2](\text{OTf})_3$  (**3**) and treated it with one equivalent of base yielding **2**. The structures of **3** were characterized by X-ray crystallography. Compound **2** also exhibits a low-spin iron(III) rhombic signal ( $g = 1.97, 2.11, 2.23$ ) in DMF at 77 K. Variable temperature magnetic susceptibility measurements indicate that **3** undergoes gradual spin increase from 2 to 400 K. DFT studies indicate that the deprotonated nitrogen in **2** forms a bond to iron(III) exhibiting double-bond character (Fe–N, 1.807 Å).

## Introduction

Hydrogen atom transfer (HAT) reactions are those wherein both a proton and electron are transferred.<sup>[1]</sup> Such a mechanism avoids the generation of high-energy intermediates.<sup>[2]</sup> HAT reactions may also be viewed as a more general proton-coupled electron transfer (PCET).<sup>[3]</sup> These reactions have been increasingly observed in reactions catalyzed by metalloenzymes.<sup>[1b,4]</sup> Examples of PCET in biological systems include lipoxygenases,<sup>[5]</sup> oxalate decarboxylase,<sup>[6]</sup> photosystem II,<sup>[7]</sup> cytochrome *c* oxidase,<sup>[8]</sup> cytochrome P450,<sup>[9]</sup> methane monooxygenases,<sup>[10]</sup> and ribonucleotide reductases.<sup>[11]</sup> Previous studies using  $[\text{Fe}^{\text{II}}(\text{H}_2\text{bip})]^{2+}$  and  $[\text{Fe}^{\text{II}}(\text{H}_2\text{bim})]^{2+}$  [ $\text{H}_2\text{bip}$  = 2,2'-bi(tetrahydropyrimidine);  $\text{H}_2\text{bim}$  = 2,2'-bi-2-imidazoline] and TEMPO (2,2,6,6-tetramethyl-1-piperidinyloxy) [Equation (1) and Equation (2)], have demonstrated this type of reaction in iron-containing model complexes.<sup>[1a,1f,4a,12]</sup>



[a] Department of Chemistry, Oakland University,  
Rochester, MI 48309-4477, USA  
E-mail: chavez@oakland.edu

[b] Biomedical Mass Spectrometry Facility, University of Michigan,  
Ann Arbor, MI 48109-0632, USA

[c] Department of Physics and Astronomy, Michigan State University,  
East Lansing, MI 48824-1322, USA

[d] Department of Chemistry, Michigan State University,  
East Lansing, MI 48824-1044, USA

Supporting information and ORCID(s) from the author(s) for this article are available on the WWW under <https://doi.org/10.1002/ejic.201701190>.

In this work we report a PCET reaction which takes place upon heating of  $[\text{Fe}^{\text{II}}(\text{tacn})_2](\text{OTf})_2$  (**1**) (tacn = 1,4,7-triazacyclononane)<sup>[13]</sup> under dynamic vacuum. The loss of an H atom from the complex results in formal oxidation of the iron(II) center to iron(III) and the generation of  $[\text{Fe}^{\text{III}}(\text{tacn})(\text{tacn-H})]^{2+}$  (**2**), where tacn-H = *N*-deprotonated tacn. We discuss the spectroscopic properties of **2** along with the synthesis and characterization of  $[\text{Fe}^{\text{III}}(\text{tacn})_2](\text{OTf})_3$  (**3**) and subsequent conversion of **3** to **2** through reaction with base. Theoretical (DFT) studies for **3** and **2** are also presented.



by a stopcock. After heating the reaction flask containing 500 mg of **1** for 3 days under static vacuum at 400 K, we closed the stopcock and heated the 50 mL to 265 °C for 24 h. Two control experiments were also conducted under the same conditions. The negative control lacked compound **1**, and 50 mL of dry H<sub>2</sub> gas was added to the positive control. After heating the flasks were then cooled to 25 °C and taken into a glovebox. To the flasks was added 1.0 mL of anhydrous [D<sub>6</sub>]DMSO. The flasks were then stoppered and shaken. The results of this experiment are shown in Figure 4. The results clearly indicate the formation of water, which is consistent with the formation of hydrogen gas during the heating of **1** under vacuum. A mercury film was also observed for the sample and positive control (faint in the case of the sample experiment) but not for the negative control.

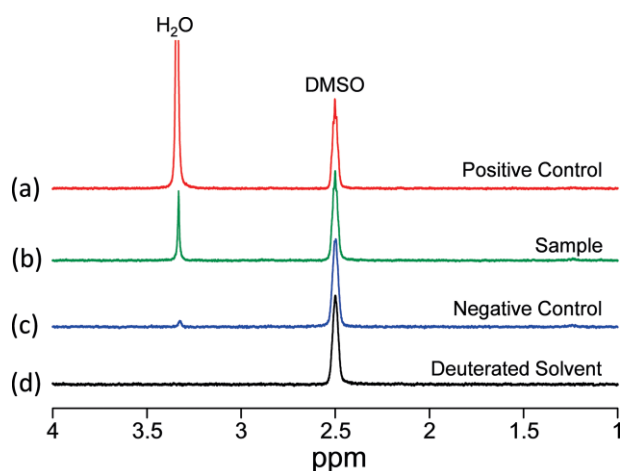


Figure 4. <sup>1</sup>H NMR spectra (25 °C) of (a) positive control (H<sub>2</sub> was heated in the presence of HgO in a closed vessel and then extracted with 1 mL of [D<sub>6</sub>]DMSO), (b) sample {headspace gas generated from heating [Fe<sup>III</sup>(tacn)<sub>2</sub>](OTf)<sub>2</sub> (**1**) under vacuum was heated in the presence of HgO in a closed vessel and then extracted with 1 mL of [D<sub>6</sub>]DMSO}, (c) negative control [same experiment as in (b) in the absence of **1**], (d) [D<sub>6</sub>]DMSO used in the experiments.

In our attempts to independently synthesize [Fe<sup>III</sup>(tacn)-(tacn-H)](OTf)<sub>2</sub> (**2**) for characterization, and to compare its properties with the thermally-induced oxidation product of **1**, we first synthesized the iron(III) analogue [Fe<sup>III</sup>(tacn)<sub>2</sub>](OTf)<sub>3</sub> (**3**) with the goal of deprotonating it to generate **2**.

To synthesize **3** we first prepared an iron(III) starting material {[Fe<sup>III</sup>(DMF)<sub>6</sub>](OTf)<sub>3</sub>}. This compound had not been previously reported but was found to have advantages over using commercially available Fe(OTf)<sub>3</sub> as the iron source. First, it has a larger molar mass (making it easier to weigh out) and second, it can be isolated in high purity crystalline form [unlike commercially available Fe(OTf)<sub>3</sub>, which is typically contains 10 % impurity]. Compound **3** was synthesized by reacting [Fe<sup>III</sup>(DMF)<sub>6</sub>](OTf)<sub>3</sub> with two equivalents of tacn in methanol. Diffusion of ether afforded bright orange crystals of **3** in good yield. UV/Vis measurements in methanol and acetonitrile yielded similar spectra, with peaks near 335 nm (400 M<sup>-1</sup> cm<sup>-1</sup>), 430 nm (100 M<sup>-1</sup> cm<sup>-1</sup>), and 513 nm (50 M<sup>-1</sup> cm<sup>-1</sup>). These bands are consistent with those observed for other iron(III) complexes.<sup>[15]</sup>

### X-ray Crystallography

The X-ray structure of **3** was determined. The crystallographic parameters for **3** are given in Table 1, whereas Table 2 contains bond lengths and angles. The structure of **3** is shown in Figure 5. The iron(III) center is coordinated by two tacn ligands in a tridentate fashion and possesses distorted octahedral geometry. Fe–N bond lengths were found to range between 1.99–

Table 1. Crystallographic data and refinement results for [Fe<sup>III</sup>(tacn)<sub>2</sub>](OTf)<sub>3</sub> (**3**).

Formula	C <sub>19</sub> H <sub>43</sub> F <sub>9</sub> FeN <sub>6</sub> O <sub>12</sub> S <sub>3</sub>
fw [g mol <sup>-1</sup> ]	870.62
Temperature [K]	173.15
Crystal system	monoclinic
Space group	<i>P</i> <sub>2</sub> <sub>1</sub> / <i>n</i>
<i>a</i> [Å]	9.0622(6)
<i>b</i> [Å]	28.8446(19)
<i>c</i> [Å]	13.6738(9)
<i>α</i> [°]	90
<i>β</i> [°]	94.5010(10)
<i>γ</i> [°]	90
Volume [Å <sup>3</sup> ]	3563.2(4)
<i>Z</i>	4
<i>Q</i> <sub>calc</sub> [Mg m <sup>-3</sup> ]	1.623
GO F	1.054
Final <i>R</i> indices [ <i>I</i> > 2σ( <i>I</i> )]	<i>R</i> 1 = 0.0611, <i>wR</i> 2 = 0.1505

Table 2. Selected bond lengths and angles of [Fe<sup>III</sup>(tacn)<sub>2</sub>](OTf)<sub>3</sub> (**3**). Calculated values are shown in brackets.

Bond lengths [Å]			
Fe–N(1)	2.00(3) [2.02]	Fe–N(4)	2.00(3) [2.02]
Fe–N(2)	2.00(3) [2.02]	Fe–N(5)	1.99(3) [2.01]
Fe–N(3)	1.99(3) [2.01]	Fe–N(6)	2.00(3) [2.02]
Bond angles [°]			
N(1)–Fe–N(2)	84.3(13) [84.3]	N(5)–Fe–N(2)	92.5(13) [96.2]
N(1)–Fe–N(4)	93.6(14) [94.9]	N(5)–Fe–N(3)	175.3(13) [179.2]
N(3)–Fe–N(1)	84.9(13) [83.0]	N(5)–Fe–N(4)	84.7(13) [83.0]
N(3)–Fe–N(2)	84.4(13) [83.3]	N(5)–Fe–N(6)	85.2(13) [83.3]
N(3)–Fe–N(4)	98.5(13) [97.5]	N(6)–Fe–N(1)	175.4(14) [178.8]
N(3)–Fe–N(6)	91.8(13) [96.2]	N(6)–Fe–N(2)	98.5(14) [96.5]
N(4)–Fe–N(2)	176.2(14) [178.8]	N(6)–Fe–N(4)	83.8(14) [84.3]
N(5)–Fe–N(1)	98.3(13) [97.5]		

2.00 Å which is consistent with other iron(III) compounds rich in nitrogen coordination.<sup>[16]</sup> These bond lengths are only slightly shorter than the iron(II) analogue, whereas the *trans* N–Fe–N bond angles are quite similar.<sup>[13]</sup> The structure also revealed a substantial H-bonding network involving the N–H groups and the triflate groups. Methanols are also involved in this bonding network (Figure 5).

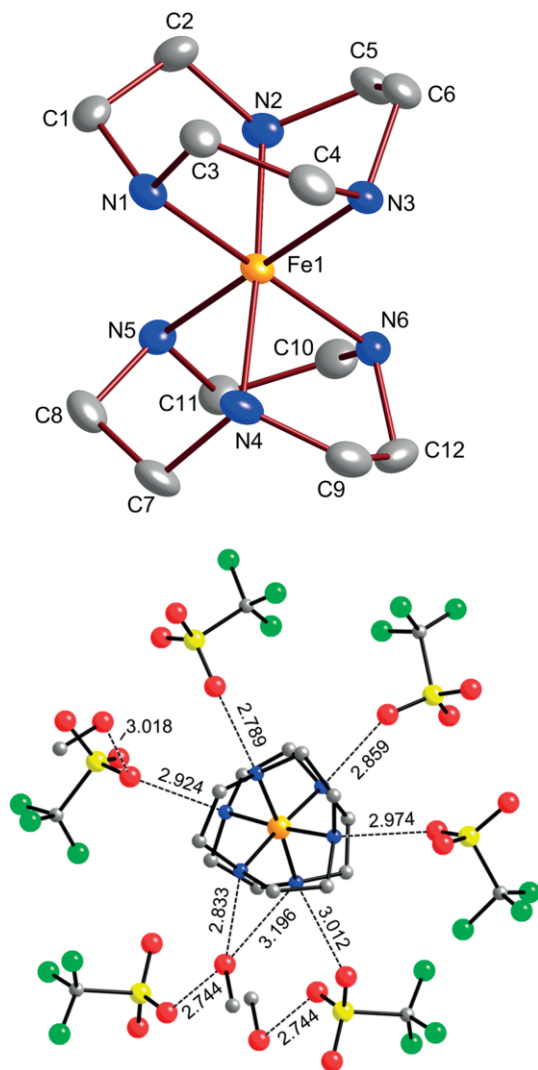


Figure 5. (Top) X-ray structure (50 % thermal ellipsoids) of  $[\text{Fe}^{\text{III}}(\text{tacn})_2](\text{OTf})_3$  (**3**) with H atoms omitted for clarity. The H-bonding network (broken lines) is also shown.

### Synthesis and Characterization of $[\text{Fe}^{\text{III}}(\text{tacn})(\text{tacn-H})](\text{OTf})_2$ (**2**)

Under dry nitrogen, **3** was treated with one equivalent of base (NaH) in DMF [Equation (4)]. Compound **2** in DMF clearly displayed a rhombic ( $g = 1.97, 2.11, 2.23$ ) low spin  $\text{Fe}^{\text{III}}$  signal (Figure 6) confirming that the +3 oxidation state remained after deprotonation. In Wieghardt's work, reaction of base with  $\{[\text{Fe}^{\text{III}}(\text{tacn})_2](\text{ClO}_4)_3\}$  was found to afford the *N*-deprotonated analogue in aqueous media as well.<sup>[17]</sup>

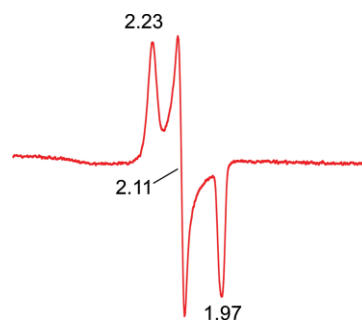
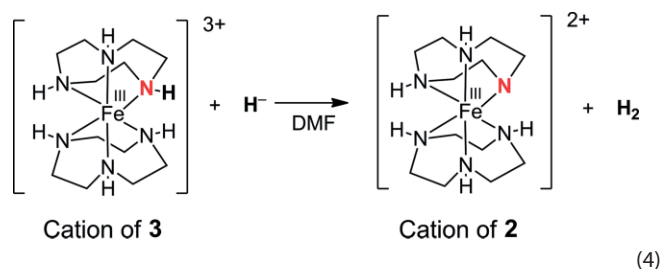


Figure 6. X-band EPR spectrum (77 K) of **2** generated by deprotonation of **3** in DMF. Selected  $g$  values are indicated. Spectrometer settings: microwave frequency 9.3 GHz; microwave power, 0.22 mW (30 dB); modulation frequency, 100 kHz; modulation amplitude, 8 G; gain,  $1 \times 10^4$ .

### Magnetic Measurements

Variable temperature SQUID measurements were performed on **3**, and show a temperature-dependent magnetization (Figure 7). At 2 K,  $\chi_M T$  has a value of  $0.46 \text{ cm}^3 \text{ mol}^{-1} \text{ K}$  ( $H = 0.1 \text{ T}$ ), which is close to the spin-only theoretical value of  $0.38 \text{ cm}^3 \text{ mol}^{-1} \text{ K}$  for low-spin  $\text{Fe}^{\text{III}}$  ( $S = 1/2$ ). As the temperature increases to 400 K, the value becomes around  $0.73 \text{ cm}^3 \text{ mol}^{-1} \text{ K}$ , which corresponds to 1.6 unpaired electrons. The Evan's NMR method<sup>[18]</sup> for solution magnetic susceptibility was performed on **3** at 298 K, and the  $\chi_M T$  values of  $0.6 \text{ cm}^3 \text{ mol}^{-1} \text{ K}$  (MeCN) and  $0.7 \text{ cm}^3 \text{ mol}^{-1} \text{ K}$  (MeOH) were determined. These values are in line with the solid state value at 300 K ( $\chi_M T = 0.66 \text{ cm}^3 \text{ mol}^{-1} \text{ K}$ ). Previously Wieghardt and co-workers prepared  $[\text{Fe}^{\text{III}}(\text{tacn})_2]\text{Cl}_3 \cdot 5\text{H}_2\text{O}$ <sup>[16h]</sup> and  $[\text{Fe}^{\text{III}}(\text{tacn})_2]\text{Br}_3 \cdot 5\text{H}_2\text{O}$ .<sup>[15]</sup>  $[\text{Fe}^{\text{III}}(\text{tacn})_2]\text{Br}_3 \cdot 5\text{H}_2\text{O}$  possesses  $\chi_M T = 0.66 \text{ cm}^3 \text{ mol}^{-1} \text{ K}$  at 20 °C suggesting a low-spin state,

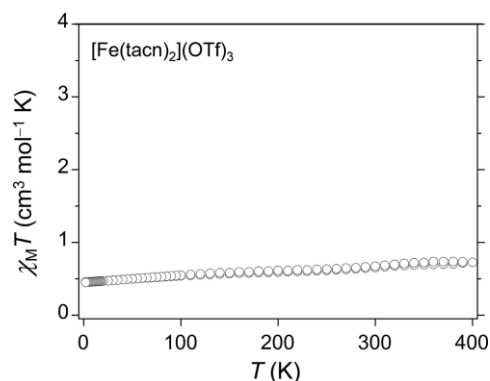


Figure 7. Temperature dependence of  $\chi_M T$  ( $H = 0.1 \text{ T}$ ) for  $[\text{Fe}^{\text{III}}(\text{tacn})_2](\text{OTf})_3$  (**3**).



however, to date no solid-state variable temperature magnetic data has been reported for either compound.

### Theoretical Calculations

DFT unrestricted calculations were carried out on complexes **2** and **3**. Ground state geometries were fully optimized in the absence of solvent. Orbital energies were calculated using PBE0/6-31G(d). A comparison between the experimental and theoretical bond lengths and angles (Table 2) for **3** showed close agreement. The greatest difference between the experimental and calculated Fe–N bond lengths are 0.02 Å for **3**, respectively. The experimental and calculated N–Fe–N bond angles are also in good agreement. Given the close agreement, the calculated values represent good approximations, and therefore the electronic properties for **3** can be confidently inferred. Furthermore, we can deduce high confidence in the calculated values for **2**. Figure 8 and Figure 9 show the following molecular orbitals: HOMO, HOMO–1, LUMO, and LUMO+1 for complexes **3** and **2**, respectively.

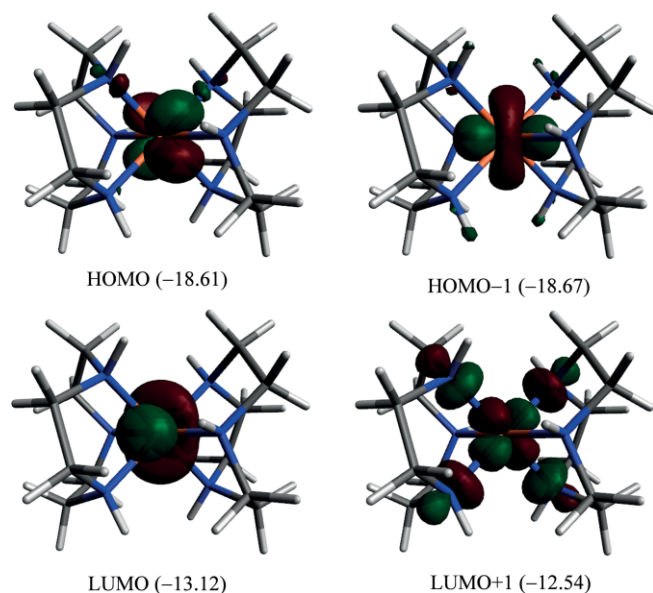


Figure 8. Plots of molecular orbitals: HOMO–1, HOMO, LUMO, and LUMO+1 for  $[\text{Fe}^{\text{III}}(\text{tacn})_2]^{3+}$  (cation of **3**). Orbital energies (eV) are indicated.

For **3** (Figure 8) it is seen that the highest occupied molecular orbital (HOMO,  $\beta$ -83) is largely distributed over the Fe  $d_{xz}/d_{yz}$  orbital. HOMO–1 ( $\beta$ -82) is also comprised of Fe  $d_{xz}/d_{yz}$ . The energies for HOMO and HOMO–1 are very close indicating near degeneracy in the optimized structure. The lowest unoccupied molecular orbital (LUMO,  $\beta$ -84) is primarily distributed over the Fe  $d_{z^2}$  orbital with very little contribution from the ligands. The metal  $d_{x^2-y^2}$  orbital are associated with LUMO+1 ( $\alpha$ -85) along with nitrogen  $p$  orbitals in an antibonding fashion. For complex **2**, (Figure 9), the HOMO ( $\alpha$ -84) is an antibonding combination between the Fe  $d_{xz}/d_{yz}$  and the N-unhybridized  $p$  orbital. The HOMO–1 ( $\beta$ -83), on the other hand is a  $\pi$ -bonding molecular orbital signifying double-bond character (Fe=N) between the

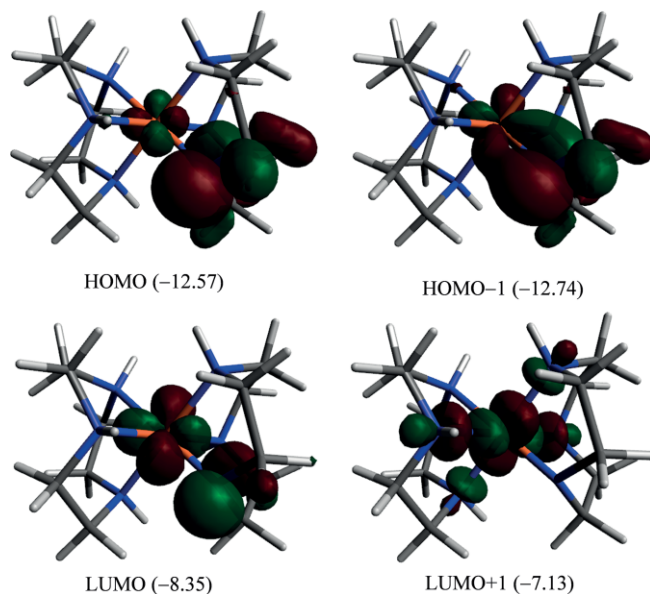


Figure 9. Plots of molecular orbitals: HOMO–1, HOMO, LUMO, and LUMO+1 for  $[\text{Fe}^{\text{III}}(\text{tacn})(\text{tacn-H})]^{2+}$  (cation of **2**). Orbital energies (eV) are indicated.

iron and nitrogen. This bond is also significantly shorter (1.807 Å) compared to the Fe–N bonds in Table 2 and the remaining Fe–N bonds in **2** (Average: 2.03 Å).

The LUMO ( $\beta$ -84) is an antibonding combination between the Fe  $d_{xz}/d_{yz}$  and the N unhybridized  $p$  orbital. LUMO+1 ( $\alpha$ -85) is mainly comprised of the Fe  $d_{x^2-y^2}$  orbital in an antibonding configuration with N  $p$  orbitals.

The HOMO–LUMO gap for **3** (5.49 eV) is slightly larger than the same value for **2** (4.22 eV), however the absolute orbital energies for **3** (HOMO: –18.61 eV) are significantly lower than **2** (HOMO: –12.57 eV) consistent with the greater stability of **3**. Although the charge and spin density on the iron center in **3** (charge = +1.079) is slightly lower than **2** (charge = +1.125), the overall charge for **3** is greater than **2** consistent with higher stability for **3**.

### Conclusions

In conclusion, heating  $[\text{Fe}^{\text{II}}(\text{tacn})_2](\text{OTf})_2$  (**1**) in the solid state under dynamic vacuum results in oxidation of the iron(II) center to iron(III). This result has been confirmed by SQUID magnetic magnetometry, EPR, and ESI-MS. Oxidation of the iron center results from removal of an H atom from the ligand (coupling with another H atom to form  $\text{H}_2$ ) generating a deprotonated amido nitrogen bonded to iron(III). The formulation of this product is  $[\text{Fe}^{\text{III}}(\text{tacn})(\text{tacn-H})](\text{OTf})_2$  (**2**, tacn-H = monodeprotonated tacn). EPR revealed that the complex contained low-spin iron(III). In our efforts to independently synthesize **2**, we first prepared  $[\text{Fe}^{\text{III}}(\text{tacn})_2](\text{OTf})_3$  (**3**), which was structurally characterized. We then reacted **3** with NaH in DMF. This resulted in formation of the deprotonated complex **2**. Variable temperature magnetic susceptibility measurements on **3** between 2–400 K indicate that **3** undergoes a gradual increase in spin. Theoretical studies indicate that the deprotonated nitrogen in **2** forms a double bond with the iron center (Fe<sup>III</sup>=N) and that complex **3**

is more stable compared to **2**. The reactivity of **2** towards protic substrates will be investigated in future studies.

## Experimental Section

**General Considerations:** Compound **1** was prepared as described previously.<sup>[13]</sup> Pure dry solvents (acetonitrile, DMF, ether, and dichloromethane) were obtained using an Innovative Technologies Inc. Solvent Purification System. Acetonitrile was further passed through activated alumina immediately prior to use. Methanol was distilled from magnesium methoxide under a nitrogen atmosphere and stored over 3 Å molecular sieves. All air sensitive manipulations were performed using standard Schlenk techniques or in a nitrogen-filled glovebox. The ligand tacn was synthesized using a literature method.<sup>[19]</sup> Elemental Analysis was performed on pulverized crystalline samples heated (40 °C) under vacuum and sealed in a glass ampule prior to submission to Atlantic Microlabs, Inc., Norcross, GA.

### Synthesis

**[Fe<sup>III</sup>(DMF)<sub>6</sub>](OTf)<sub>3</sub>:** Under nitrogen, FeCl<sub>3</sub> (555.5 mg, 3.45 mmol) was dissolved in CH<sub>3</sub>CN (2 mL) and CH<sub>2</sub>Cl<sub>2</sub> (4 mL) and stirred. Me<sub>3</sub>SiOTf (2.556 g, 11.5 mmol) was added to the stirring solution dropwise. The solution turned deep red and was stirred overnight. The next day the solution was placed under high vacuum and the volume was reduced to 5 mL. The solution was then filtered and DMF (1 mL) was added (note: this reaction is highly exothermic). The solution became yellow–green in color. Diethyl ether (10 mL) was added and the solution was placed in the freezer. Large yellow–green crystals were deposited overnight. These crystals were collected, washed with diethyl ether and dried under vacuum. Yield: 2.65 g (79.6 %). Elemental analysis for C<sub>21</sub>H<sub>42</sub>F<sub>9</sub>FeN<sub>6</sub>O<sub>15</sub>S<sub>3</sub>: C, 26.79; H, 4.50; N, 8.93; found C, 27.24; H, 4.43; N, 9.35.

**[Fe<sup>III</sup>(tacn)<sub>2</sub>](OTf)<sub>3</sub> (**3**):** In a nitrogen-filled glovebox, tacn (100 mg, 0.410 mmol) was dissolved in MeOH (1 mL). [Fe<sup>III</sup>(DMF)<sub>6</sub>](OTf)<sub>3</sub> (364.9 mg, 0.20 mmol) was dissolved in MeOH (2 mL). The tacn solution was added dropwise to the stirring [Fe<sup>III</sup>(DMF)<sub>6</sub>](OTf)<sub>3</sub> solution and stirred overnight. The solution was then filtered and placed in a diethyl ether chamber affording red–orange crystals after 24 h. Yield: 156 mg (58 %) IR (KBr pellet) [ $\tilde{\nu}$ , cm<sup>-1</sup>]: 3522 (w), 3249 (w), 3083 (m), 2855 (w), 2796 (w), 2315 (w), 1661 (s), 1483 (w), 1458 (w), 1434 (w), 1396 (w), 1252 (s), 1165 (s), 1111 (w), 1031 (m), 986 (w), 839 (w), 817 (w), 763 (w), 639 (m), 577 (w), 519 (w), 485 (w). UV/Vis (CH<sub>3</sub>OH) [ $\lambda_{\text{max}}$ , nm ( $\epsilon$ , M<sup>-1</sup> cm<sup>-1</sup>)]: 230 (22,000, sh), 281 (5,200, sh), 338 (356), 433 (105), 513 (45, sh). UV/Vis (CH<sub>3</sub>CN) [ $\lambda_{\text{max}}$ , nm ( $\epsilon$ , M<sup>-1</sup> cm<sup>-1</sup>)]: 252 (21,300), 333 (428), 432 (129), 513 (57, sh). UV/Vis (DMF) [ $\lambda_{\text{max}}$ , nm ( $\epsilon$ , M<sup>-1</sup> cm<sup>-1</sup>)]: 340 (581), 432 (162), 520 (66, sh). Elemental analysis for C<sub>15</sub>H<sub>30</sub>F<sub>9</sub>FeN<sub>6</sub>O<sub>9</sub>S<sub>3</sub>: C, 23.66; H, 3.97; N, 11.04; found C, 23.65; H, 3.98; N, 10.91.

**Physical Measurements:** <sup>1</sup>H NMR spectra were recorded at 25 °C on a Bruker Avance II 400 MHz instrument and sample peaks in [D<sub>2</sub>]dichloromethane were referenced to TMS (tetramethylsilane). FT-IR spectra were measured on a Varian 3100 Excalibur Series. Optical spectra were collected on a Cary 50 UV/Vis spectrophotometer. EPR spectra were recorded on a Varian Century series X-band (9.3 GHz) device with an E-4531 dual-cavity 9 inch magnet and a 200 mW Klystron. Special recording was carried out on ESRTAK software. All EPR spectra were recorded at 77 K. A 1 mm Cu complex<sup>[20]</sup> in DMF was used as a standard to calculate the spins and *g* values in the *g* ≈ 2 region, and a 1 mm Fe<sup>III</sup>/EDTA solution [prepared by stirring FeCl<sub>3</sub>·6H<sub>2</sub>O with excess Na<sub>2</sub>EDTA·2H<sub>2</sub>O (Aldrich) for several hours] was used to calculate the spins and *g* values in the *g* ≈ 4.3

region. ESI-MS experiments were performed on a Thermo Finnigan TSQ Quantum Ultra AM triple quadrupole mass spectrometer.

**X-ray Crystallography:** [Fe<sup>III</sup>(tacn)<sub>2</sub>](OTf)<sub>3</sub> (**3**) was crystallized by diffusion of diethyl ether into a methanol solution of **3**. An orange-red plate crystal with dimensions 0.53 × 0.35 × 0.15 mm<sup>3</sup> was mounted on a Nylon loop using very small amount of paratone oil. Data were collected using a Bruker CCD (charge-coupled device) based diffractometer equipped with an Oxford Cryostream low-temperature apparatus operating at 173 K. Data were measured using  $\omega$  and  $\varphi$  scans of 0.5° per frame for 30 s. The total number of images was based on results from the program COSMO<sup>[21]</sup> where redundancy was expected to be 4.0 and completeness to 0.83 Å to 100 %. Cell parameters were retrieved using APEX II software<sup>[22]</sup> and refined using SAINT on all observed reflections. Data reduction was performed using the SAINT software<sup>[23]</sup> which corrects for Lp. Scaling and absorption corrections were applied using SADABS<sup>[24]</sup> multi-scan technique, supplied by George Sheldrick. The structures are solved by the direct method using the SHELXS-97 program and refined by least-squares method on *F*<sup>2</sup>, SHELXL-97,<sup>[25]</sup> which are incorporated in OLEX2.<sup>[25]</sup> The structure was solved in the space group *P2*<sub>1</sub>/*n* (no. 14). All non-hydrogen atoms are refined anisotropically. Hydrogens were calculated by geometrical methods and refined as a riding model. Although there is disorder in one of the anions, (SO<sub>3</sub>CF<sub>3</sub>)<sup>-</sup>, modeling of this disordered failed to yield chemical and crystallographic correct models and therefore no disorder model is provided here, although there is a large electron density peak within the anion. All drawings are done at 50 % ellipsoids. Please refer to Table 1 for additional crystal and refinement information.

CCDC 1406004 (for **3**) contains the supplementary crystallographic data for this paper. These data can be obtained free of charge from The Cambridge Crystallographic Data Centre.

**Magnetic Measurements:** Variable temperature magnetic susceptibilities were measured using a Quantum Design MPMS SQUID magnetometer calibrated with a 765-Palladium standard purchased from NIST (formally NSB). Powdered samples were placed in plastic bags. Samples were measured in the temperature range 2–400 K (*H* = 0.1 T). The magnetic contribution of the bags was subtracted from the sample. Samples were placed in plastic straws for measurements. The molar magnetic susceptibilities were corrected for the diamagnetism of the complexes using tabulated values of Pascal's constants to obtain a corrected molar susceptibility. Solution magnetic susceptibility was determined using the Evan's Method (<sup>1</sup>H NMR) at 298 K.<sup>[18]</sup> The mass susceptibility ( $\chi_g$ ) was calculated using Equation (5):

$$\chi_g = \frac{-3\Delta f}{4\pi f m} + \chi_o \left[ 1 + \frac{(d_o - d_s)}{m} \right] \quad (5)$$

Where  $\Delta f$  is the frequency shift in Hz of the reference compound, *f* is the fixed probe frequency of spectrometer,  $\chi_o$  is the mass susceptibility in 1 mL of solution, and *d<sub>o</sub>* and *d<sub>s</sub>* are the densities of the solvent and solution, respectively.

**Computational Details:** Quantum chemical calculations providing energy minimized molecular geometries, molecular orbitals (HOMO–LUMO), and vibrational spectra for compound **2** and **3** were carried out using density functional theory (DFT) as implemented in the GAUSSIAN09 (Revision C.01) program package.<sup>[26]</sup> We employed the hybrid functional PBE0<sup>[27]</sup> containing 25 % of exact exchange. We employed the basis set 6-31G(d).<sup>[28]</sup> Full ground state geometry optimization was carried out without any symmetry constraints. Only the default convergence criteria were used during the

geometry optimizations. The initial geometry was taken from the crystal structure coordinates in the doublet state. Optimized structures were confirmed to be local minima (no imaginary frequencies for both cases). Molecular Orbitals were generated using Avogadro<sup>[29]</sup> (an open-source molecular builder and visualization tool, Version 1.1.0. <http://avogadro.openmolecules.net/>).

**Supporting Information** (see footnote on the first page of this article): Tables containing crystal data for **3** (21 pages).

## Acknowledgments

Financial support from Oakland University (OU-REF) and National Science Foundation (NSF) Grant No. CHE-0748607 is gratefully acknowledged. J.L. acknowledges a graduate fellowship from OU. The National Science Foundation (NSF) award (CHE-0821487) and National Institutes of Health (NIH) award (R15GM112395) are also acknowledged. A.A. and M.D.S. thank the National Cancer Institute of the National Institutes of Health (Grant R01CA045424) for support. A.A. and M.D.S. are also grateful to Research Excellence Fund (REF) and Center for Biomedical Research (CBR) at Oakland University for support.

**Keywords:** Iron · Oxidation · EPR · Density functional calculations · Magnetic properties

- [1] a) E. A. Mader, E. R. Davidson, J. M. Mayer, *J. Am. Chem. Soc.* **2007**, *129*, 5153–5166; b) E. A. Mader, V. W. Manner, T. F. Markle, A. Wu, J. A. Franz, J. M. Mayer, *J. Am. Chem. Soc.* **2009**, *131*, 4335–4345; c) J. L. Li, S. D. Zhou, J. Zhang, M. Schlangen, T. Weiske, D. Usharani, S. Shaik, H. Schwarz, *J. Am. Chem. Soc.* **2016**, *138*, 7973–7981; d) A. Pannwitz, O. S. Wenger, *Phys. Chem. Chem. Phys.* **2016**, *18*, 11374–11382; e) J. L. Li, S. D. Zhou, X. N. Wu, S. Y. Tang, M. Schlangen, H. Schwarz, *Angew. Chem. Int. Ed.* **2015**, *54*, 11861–11864; *Angew. Chem.* **2015**, *127*, 12028; f) J. M. Mayer, *Acc. Chem. Res.* **2011**, *44*, 36–46.
- [2] T. R. Porter, J. M. Mayer, *Chem. Sci.* **2014**, *5*, 372–380.
- [3] a) T. V. Chciuik, W. R. Anderson, R. A. Flowers, *J. Am. Chem. Soc.* **2016**, *138*, 8738–8741; b) E. C. Gentry, R. R. Knowles, *Acc. Chem. Res.* **2016**, *49*, 1546–1556; c) T. T. Eisenhart, W. C. Howland, J. L. Dempsey, *J. Phys. Chem. B* **2016**, *120*, 7896–7905; d) H. G. Yayla, H. J. Wang, K. T. Tarantino, H. S. Orbe, R. R. Knowles, *J. Am. Chem. Soc.* **2016**, *138*, 10794–10797; e) H. Mitome, T. Ishizuka, H. Kotani, Y. Shiota, K. Yoshizawa, T. Kojima, *J. Am. Chem. Soc.* **2016**, *138*, 9508–9520.
- [4] a) J. S. Kretschmer, T. F. Miller, *Inorg. Chem.* **2016**, *55*, 1022–1031; b) H. M. Neu, R. A. Baglia, D. P. Goldberg, *Acc. Chem. Res.* **2015**, *48*, 2754–2764.
- [5] A. V. Soudackov, S. Hammes-Schiffer, *J. Phys. Chem. Lett.* **2014**, *5*, 3274–3278.
- [6] B. T. Saylor, L. A. Reinhardt, Z. B. Lu, M. S. Shukla, L. Nguyen, W. W. Cleland, A. Angerhofer, K. N. Allen, N. G. J. Richards, *Biochemistry* **2012**, *51*, 2911–2920.
- [7] a) T. Irebo, S. Y. Reece, M. Sjödin, D. G. Nocera, L. Hammarstrom, *J. Am. Chem. Soc.* **2007**, *129*, 15462–15464; b) A. R. Offenbacher, L. A. Burns, C. D. Sherrill, B. A. Barry, *J. Phys. Chem. B* **2013**, *117*, 8457–8468; c) D. J. Stewart, M. K. Brennaman, S. E. Bettis, L. Wang, R. A. Binstead, J. M. Papanikolas, T. J. Meyer, *J. Phys. Chem. Lett.* **2011**, *2*, 1844–1848.
- [8] M. R. A. Blomberg, P. E. M. Siegbahn, *Biochim. Biophys. Acta* **2006**, *1757*, 969–980.
- [9] a) H. Hirao, P. Chuanpravit, *Chem. Phys. Lett.* **2015**, *621*, 188–192; b) Y. Wang, H. Hirao, H. Chen, H. Onaka, S. Nagano, S. Shaik, *J. Am. Chem. Soc.* **2008**, *130*, 7170–7171.
- [10] a) D. Wang, L. Que, *Chem. Commun.* **2013**, *49*, 10682–10684; b) M. Merckx, D. A. Kopp, M. H. Sazinsky, J. L. Blazyk, J. Muller, S. J. Lippard, *Angew. Chem. Int. Ed.* **2001**, *40*, 2782–2807; *Angew. Chem.* **2001**, *113*, 2860.
- [11] L. Olshansky, B. L. Greene, C. Finkbeiner, J. Stubbe, D. G. Nocera, *Biochemistry* **2016**, *55*, 3234–3240.
- [12] J. P. Roth, J. C. Yoder, T. J. Won, J. M. Mayer, *Science* **2001**, *294*, 2524–2526.
- [13] A. S. Tolla, A. Banerjee, S. Stjepanovic, J. Li, W. W. Brennessel, R. Loloee, F. A. Chavez, *Eur. J. Inorg. Chem.* **2013**, 2115–2121.
- [14] a) A. Jordan, B. Steinberg, *Atmos. Meas. Technol.* **2011**, *4*, 509–521; b) T. Kawano, N. Tsuboi, H. Tsujii, T. Sugiyama, Y. Asakura, T. Uda, *J. Chromatogr. A* **2004**, *1023*, 123–127.
- [15] K. Wieghardt, W. Schmidt, W. Herrmann, *Inorg. Chem.* **1983**, *22*, 2953–2956.
- [16] a) T. Fujinami, K. Nishi, R. Kitashima, K. Murakami, N. Matsumoto, S. Iijima, K. Toriumi, *Inorg. Chim. Acta* **2011**, *376*, 136–143; b) D. J. Harding, D. Sertphon, P. Harding, K. S. Murray, B. Moubarak, J. D. Cashion, H. Adams, *Chem. Eur. J.* **2013**, *19*, 1082–1090; c) M. Koike, K. Murakami, T. Fujinami, K. Nishi, N. Matsumoto, Y. Sunatsuki, *Inorg. Chim. Acta* **2013**, *399*, 185–192; d) M. Martinho, G. Q. Xue, A. T. Fiedler, L. Que, E. L. Bominaar, E. Munck, *J. Am. Chem. Soc.* **2009**, *131*, 5823–5830; e) D. Sertphon, D. J. Harding, P. Harding, K. S. Murray, B. Moubarak, J. D. Cashion, H. Adams, *Eur. J. Inorg. Chem.* **2013**, 788–795; f) C. F. Sheu, S. M. Chen, G. H. Lee, Y. H. Liu, Y. S. Wen, J. J. Lee, Y. C. Chuang, Y. Wang, *Eur. J. Inorg. Chem.* **2013**, 894–901; g) A. Tissot, P. Fertey, R. Guillot, V. Briois, M. L. Boillot, *Eur. J. Inorg. Chem.* **2014**, 101–109; h) J. C. A. Boeyens, A. G. S. Forbes, R. D. Hancock, K. Wieghardt, *Inorg. Chem.* **1985**, *24*, 2926–2931.
- [17] K. Pohl, K. Wieghardt, W. Kaim, S. Steenken, *Inorg. Chem.* **1988**, *27*, 440–447.
- [18] C. Piguet, *J. Chem. Educ.* **1997**, *74*, 815–816.
- [19] G. H. Searle, R. J. Geue, *Aust. J. Chem.* **1984**, *37*, 959–970.
- [20] A. Y. S. Malkhasian, M. E. Finch, B. Nikolovski, A. Menon, B. E. Kucera, F. A. Chavez, *Inorg. Chem.* **2007**, *46*, 2950–2952.
- [21] COSMO V1.61, Software for the CCD Detector Systems for Determining Data Collection Parameters. Bruker Analytical X-ray Systems, Madison, WI (2009).
- [22] APEX2 V2010.11–3. Software for the CCD Detector System; Bruker Analytical X-ray Systems, Madison, WI (2010).
- [23] SAINT V 7.68A Software for the Integration of CCD Detector System Bruker Analytical X-ray Systems, Madison, WI (2010).
- [24] SADABS V2008/2 Program for absorption corrections using Bruker-AXS CCD based on the method of Robert Blessing; R. H. Blessing, *Acta Crystallogr., Sect. A* **1995**, *51*, 33–38.
- [25] “A short history of SHELX”. G. M. Sheldrick, *Acta Crystallogr., Sect. A* **2008**, *64*, 112–122.
- [26] M. J. Frisch, G. W. Trucks, H. B. Schlegel, G. E. Scuseria, M. A. Robb, J. R. Cheeseman, G. Scalmani, V. Barone, B. Mennucci, G. A. Petersson, H. Nakatsuji, M. Caricato, X. Li, H. P. Hratchian, A. F. Izmaylov, J. Bloino, G. Zheng, J. L. Sonnenberg, M. Hada, M. Ehara, K. Toyota, R. Fukuda, J. Hasegawa, M. Ishida, T. Nakajima, Y. Honda, O. Kitao, H. Nakai, T. Vreven, J. A. Montgomery Jr., J. E. Peralta, F. Ogliaro, M. Bearpark, J. J. Heyd, E. Brothers, K. N. Kudin, V. N. Staroverov, R. Kobayashi, J. Normand, K. Raghavachari, A. Rendell, J. C. Burant, S. S. Iyengar, J. Tomasi, M. Cossi, N. Rega, J. M. Millam, M. Klene, J. E. Knox, J. B. Cross, V. Bakken, C. Adamo, J. Jaramillo, R. Gomperts, R. E. Stratmann, O. Yazyev, A. J. Austin, R. Cammi, C. Pomelli, J. W. Ochterski, R. L. Martin, K. Morokuma, V. G. Zakrzewski, G. A. Voth, P. Salvador, J. J. Dannenberg, S. Dapprich, A. D. Daniels, Ö. Farkas, J. B. Foresman, J. V. Ortiz, J. Cioslowski, D. J. Fox, *Gaussian 09, Revision C.01*, Gaussian, Inc., Wallingford CT, **2010**.
- [27] C. Adamo, V. Barone, *J. Chem. Phys.* **1999**, *110*, 6158–6170.
- [28] G. A. Petersson, M. A. Al-Laham, *J. Chem. Phys.* **1991**, *94*, 6081–6090.
- [29] M. Hanwell, D. Curtis, D. Lonie, T. Vandermeersch, E. Zurek, G. Hutchison, *J. Cheminf.* **2012**, *4*, 1–17.

Received: October 6, 2017